

Research Article

Magnetorheological Smart Automotive Engine Mount

Chiranjit Sarkar^{†*}, Harish Hirani[‡] and Abhijit Sasane[¶]

[†]Mechanical Engineering Department, Delhi Technological University, Shahbad Daluapur, Bawana Road, Delhi – 110042, India

[‡]Mechanical Engineering Department, Indian Institute of Technology Delhi, Hauz Khas, New Delhi – 110016, India

[¶]Senior Manager, Tata Motors, Mumbai, India

Accepted 18 Feb 2015, Available online 20 Feb 2015, Vol.5, No.1 (Feb 2015)

Abstract

An ideal engine mount system isolates vibrations caused by engine dynamic disturbances in various speed ranges, and prevents engine bounce originated by shock excitations. The stiffness and damping of the ideal engine mount are functions of the frequency and amplitude of vibration. To avoid transmission of medium to high frequency and low amplitude vibrations, an idle engine mount should be 'Soft' (low dynamic stiffness). On the other hand, road excitations passing through the tires and vehicle suspension system cause the structural- vibrations of low frequency and high amplitude. To deal with this case, an idle engine mount should be 'Stiff' (high dynamic stiffness). Such contradictory requirements from an engine mount demands engine mount to be smart. The aim of the present paper is to target a smart mount which will perform similar to Ideal mount. The present paper proposes MRF mount to provide variable dynamic stiffness characteristics. A theoretical design of MRF mount system has been sketched and performance evaluation of MR mount approaching to the ideal engine mount has been presented.

Keywords: Comparative study among engine mounts, Active engine mount, Ideal engine mount, Magnetorheological engine mount.

1. Introduction

Internal combustion engines are commonly used in automobile industries to produce the required driving power. The firing pulse in the engine-cylinders; and the inertia force and torque caused by the rotating and reciprocating parts (i.e. piston, connecting rod, and crank) generate engine dynamic disturbances. Frequency and amplitude of such disturbances for 4 cylinder-four stroke engine range between 30Hz to 250 Hz, and 0.1mm to 0.5mm respectively (Bernuchon, 1984). These disturbances increase the level of noise and vibrations of automobile structure. Further, objectives of engine-weight-minimization (Yu, *et al*, 2001) and engine-power-maximization lead an engine design of higher levels of vibration and noise (Singh, 2000). On the other hand, modern automobile industries (Yu, *et al*, 2001) are targeting the passengers' comfort, which is inversely proportional to noise and vibrations of automobile structure. To resolve these conflicting requirements, an engine mounting system is designed to bear the engine-weight and to isolate the unbalanced engine disturbance from transmission to the vehicle structure. To avoid transmission of medium to high frequency and low amplitude vibrations, an idle engine mount should be 'Soft' (low dynamic stiffness). On the other hand, road excitations passing through

the tires and vehicle suspension system, cause the structural- vibrations of low frequency (0-30 Hz) and high amplitude (0.5mm to 1.5mm) at engine mount locations (Patrick and Ticks, 1984). To deal with such low-frequency and high-amplitude-vibrations, an idle engine mount should be 'Stiff' (high dynamic stiffness) to carry the engine along with chassis without any relative movement between them. In additions to these requirements from an idle engine mount, a special need arises during idling of engine, which imparts low-frequency and low-amplitude vibrations. To isolate chassis from such low frequency and low-amplitude vibrations, engine mount should show its 'soft' behaviour. Thus the dynamic characteristics of the mount, which is expressed as complex number, should vary along with the frequency and amplitude of vibrations. The magnitude of this complex number is named 'Dynamic Stiffness'. For an ideal mount the dynamic stiffness is characterized by the curve as shown in Fig.1. In this figure, red dotted lines demonstrate the behaviour of an ideal mount considering the low frequency high amplitude (road excitations), low frequency low amplitude (engine idling) and high frequency low amplitude (engine) vibrations. Unfortunately available engine mounts such as elastomeric/rubber mount (Regis, 1976), hydraulic mount with orifice (Concoran and Ticks, 1984), hydraulic mount with inertia track (Flower, 1985), and hydraulic mount with inertia track and decoupler

*Corresponding author: Chiranjit Sarkar

(Ushijima, 1988) do not meet the “ideal required dynamic stiffness”. Therefore the present proposes a novel engine mount system, performance of which approaches to the “ideal engine mount”. A systematic methodology of comparative study among available engine mounts has been presented and a need to design proposed novel Magnetorheological engine mount have been illustrated. The details of magnetorheological fluids (MRF) are available in the literature (Sarkar and Hirani, 2015), (Sarkar and Hirani, 2013), (Sukhwani, et al, 2009), (Sukhwani and Hirani, 2007), (Sukhwani and Hirani, 2008), (Sukhwani and Hirani, 2008), (Hirani and Manjunatha, 2007), (Sukhwani, et al, 2007), (Sukhwani, et al, 2006), (Gupta and Hirani, 2011), . In the present paper, design and analysis of Magnetorheological engine mount has been presented.

2. Literature Analysis

A comparative study of available engine mounts with their advantages and limitations has been described in following sub-sections.

2.1 Passive Elastomeric/Rubber Mount

Elastomeric mounts have been used to isolate vehicle structure from engine vibration since the 1930's (Regis, 1976). Gomes and Pouzada (2002) explained the effect of rubber compound formulation on the dynamic properties of elastomeric mount. To understand the behaviour of the elastomeric mount, it is often (Bernuchon, 1984), (Regis, 1976), (Choudhury, 2004), modelled as a nonlinear spring as function of the excitation frequency. One of such models provided by Rao, *et al.*(2001) is,

$$k_d = \sqrt{k^2 + (c\omega_{dr})^2} \quad (1)$$

This equation clearly indicates that dynamic stiffness (k_d) is a function of static stiffness (k), damping property (C), and operating frequency. Using the Eq. 1, the variation in the value of dynamic stiffness of elastomeric mount (for $k = 6.98e7$ N/m, and $c = 6.4e4$ Ns/m) with operating frequency is plotted in Fig. 1.

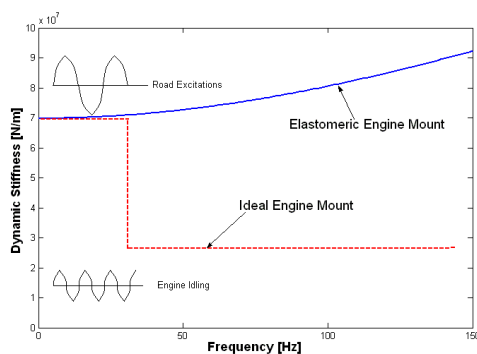


Fig.1 Dynamic Stiffness of Elastomeric Mount

On comparing (Fig. 1) this behaviour of dynamic stiffness with ideal dynamic stiffness, it can be concluded that elastomeric mount is suitable to deal with low frequency and high amplitude vibrations, but it is unable to isolate low-frequency-low amplitude and high-frequency-low-amplitude vibrations.

2.2 Hydraulic Engine Mount (HEM)

Corcoran and Ticks (1984) experimentally compared the performance of hydraulic engine mount with elastomeric mount on the basis of vibratory and acoustic comforts at operator's seat. They measured seat belt acceleration and sound power level for the comparison. They described advantages of hydraulic engine mount over elastomeric mount particularly during low frequency vibration such as engine bounce (motion of the engine with respect to chassis when vehicle is passing over bump) and idle shake (vibrations of engine when engine is in idling condition).

Three-dimensional exploded view of a typical HEM is shown in Fig.2. HEM consists of two fluid-filled chambers connected through a restricted (i.e. Orifice or narrow tubular path also termed as “inertia track”) passage. The fluid used in HEM is generally having less viscosity for ease of flow across the chambers. Based on restricted passage, hydraulic mounts can be classified as: HEM with orifice (HEM-O), HEM with Inertia track (HEM-IT) and HEM with Inertia track and Decoupler (HEM-ITD) (Flower, 1985).

Flower, (1985) explained these three hydraulic mounts (HEM-O, HEM-IT and HEM-ITD) using mechanical system models and a set of the equations. However, equations for hydraulic engine mount with inertia track and decoupler were not covered by (Flower, 1985). These equations were detailed by Ushijima, *et al.*(1988). To simplify the understanding of the HEM, low- and high- frequency approaches were described by Adiguna, *et al.*, (2003) and Kim and Singh, (1995). Adiguna, *et al.*, (2003) provided the equations of HEM-ITD in frequency domain. The details of all three HEMs are described in following subsections.

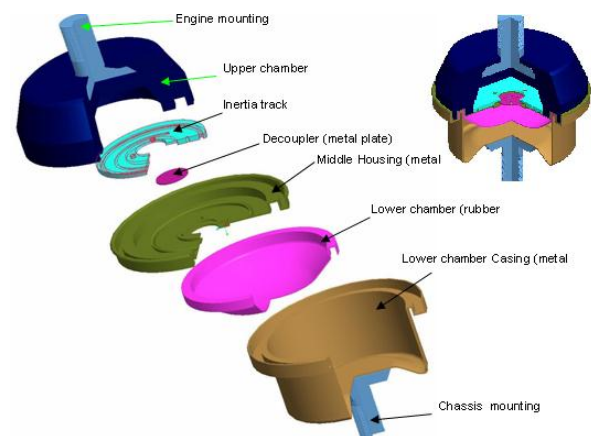


Fig.2 HEM with Inertia Track and Decoupler

2.2.1 HEM with Orifice

The orifice plate which divides the mount in two halves is made up of resilient material as shown in Fig.3a (Singh, 2007). During the operation when mounted engine cause the displacement of the upper chamber, the liquid is forced to pass through the small orifice opening from upper chamber to lower chamber or reverse. During this fluid motion, the resistance offered by the orifice is related to the amplitude of the excitation frequency. During large amplitudes (low frequencies 0 to 30 Hz) more resistance is offered and higher stiffness is exerted. Whereas during the low amplitudes (high frequencies 30 to 250 Hz) the resistance offered is less, so the stiffness is lesser. As per Flower, (1985) the characteristic equation of the HEM with orifice mount can be expressed as:

$$K(\omega_{dr}, j) = k_r + j\omega_{dr}b_r + \frac{A_p^2}{C_1} * \frac{j\omega + \frac{1}{R_o C_2}}{j\omega + \frac{1}{R_o} \left(\frac{1}{C_1} + \frac{1}{C_2} \right)} \tag{2}$$

The dynamic stiffness curve ($k_r=2.25e^5N/m$, $b_r=100Ns/m$, $A_p=0.0025m^2$, $C_1=3e^{-11}m^5/N$, $R_o=$, $C_2=2.6e^{-9}$, Amplitude =0.1mm etc.) of HEM-O is shown in fig.4.

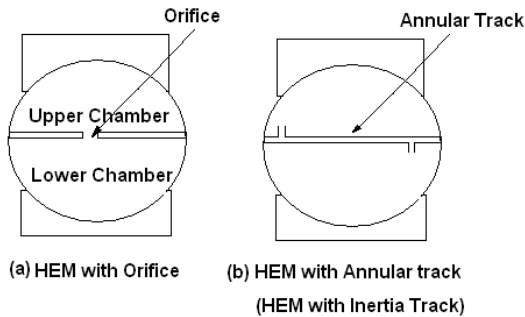


Fig.3 Schematic representation of Hydraulic mounts

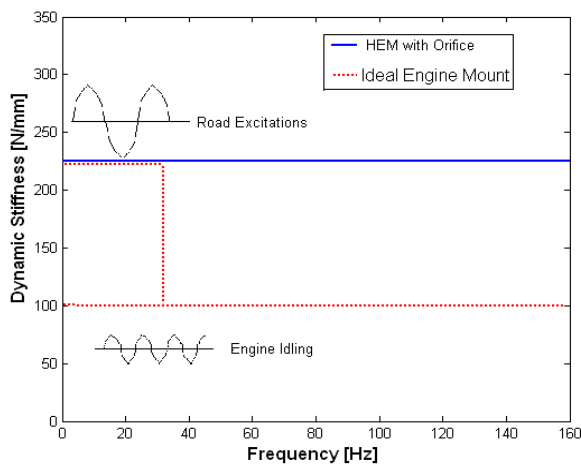


Fig.4 Dynamic Stiffness of HEM-O

Figure 4 illustrates almost constant value of the dynamic stiffness of the HEM-O mount, unlike

elastomeric mount which shows increase in dynamic stiffness with increase in operating frequency. The requirement of ideal mount plotted in Fig. 4 indicates that in higher frequency zone HEM-O deviates from ideal mount. Improvement in dynamic performance of hydraulic mount can be achieved by replacing orifice geometry with an annular track as shown in Fig. 3b. HEM with such annular track connection between two chambers is termed as “HEM with Inertia track”.

2.2.2 HEM with Inertia Track (HEM-IT)

The inertia track is a long annular pipe joining the two chambers. It is a part of a thin membrane which separates upper and lower chambers (Singh, 2000) or may be an external thin tube joining the chambers (Venezia, 1997). During the low amplitude high frequency vibrations, the displaced fluid is accommodated by thin membrane; hence HEM acts as “Soft HEM”. In case of low frequency high amplitude vibrations, the membrane cannot accommodate all the displaced volume of the fluid and fluid enters in inertia track to get transferred from one chamber to other chamber. Long length and small cross sectional area of inertia track offers reasonable resistance to fluid-flow and adds to the stiffness of the mount. As the inertia of the fluid oscillating in the track adds to the total stiffness of the mount, the track is called as inertia track (Singh, 2000). The dynamic stiffness of HEM-IT can be (Ahmadian and Kong, 1999) expressed as,

$$\text{Dynamic stiffness } K^* = |K' + K''| \tag{3}$$

where

$$K' = k_r + A_p^2 \frac{\omega_{dr}^2 [I_i \omega_{dr}^2 (k_v I_i - b_v^2) - k_v (k_v I_i - R_i^2)]}{(k_v - I_i \omega_{dr}^2)^2 + [\omega_{dr} (R_i + b_v)]^2} \tag{4}$$

$$K'' = (b_r + A_p^2 b_v) \omega_{dr} + A_p^2 \frac{\{k_v^2 (R_i - b_v) \omega_{dr} + \omega_{dr}^3 [2k_v b_v I_i - b_v^2 (R_i + b_v)]\}}{(k_v - I_i \omega_{dr}^2)^2 + [\omega_{dr} (R_i + b_v)]^2} \tag{5}$$

The term Resistance and Inertance expressed in equation 4 and 5 are given as

$$\text{Resistance} = R_i = \frac{32 \mu L_i}{A_i} \tag{6}$$

$$\text{Inertance} = I_i = \frac{\rho L_i}{A_i} \tag{7}$$

By putting these expressions of resistance and inertance from equation 6 and 7 into equation 4 and 5, the characteristic equation of dynamic stiffness in terms of Area of Inertia Track (A_i) can be expressed as,

$$K' = k_r + A_p^2 \frac{\omega_{dr}^2 [\omega_{dr}^2 \rho L_i A_i (k_v \rho L_i - A_i b_v^2) - k_v (k_v \rho L_i A_i - 1024 \mu^2 L_i^2)]}{(A_i^2 k_v - \omega_{dr}^2 \rho L_i A_i)^2 + [\omega_{dr} (32 \mu L_i + A_i b_v)]^2} \tag{8}$$

$$K'' = (b_r + A_p^2 b_v) \omega_{dr} + A_p^2 A_i \frac{\{k_v^2 (32 \mu L_i - b_v A_i) \omega_{dr} + \omega_{dr}^3 [2k_v b_v \rho L_i - b_v^2 (32 \mu L_i + b_v A_i)]\}}{(A_i^2 k_v - \omega_{dr}^2 \rho L_i A_i)^2 + [\omega_{dr} (32 \mu L_i + A_i b_v)]^2} \tag{9}$$

Using Eqs. (3-9) the dynamic stiffness curve of HEM-IT versus frequency has been plotted in Fig.5.

The Fig. 5 illustrates that during “low frequency high amplitude” and “high frequency low amplitude” vibrations, the dynamic stiffness of HEM-IT approaches to dynamic stiffness required from an ideal mount. However, such performance is restricted by “notch frequency” (Ahmadian and Kong, 1999) as indicated in Fig. 5 and this observation provide a guideline that operating frequency of vibrations need to be lesser than notch frequency so that “resonance peak (Ahmadian and Kong, 1999)”, which occurs just after notch frequency, can be avoided. This kind of HEM is better than elastomeric mount and HEM-O. However, this mount is unable to fulfil the required performance during “idle engine” conditions, as “HEM with Inertia track” shows relatively higher stiffness in lower frequency zone. In such case, engine vibrations pass to the chassis. To solve this problem, HEM with Inertia track and decoupler (Flower, 1985) was introduced.

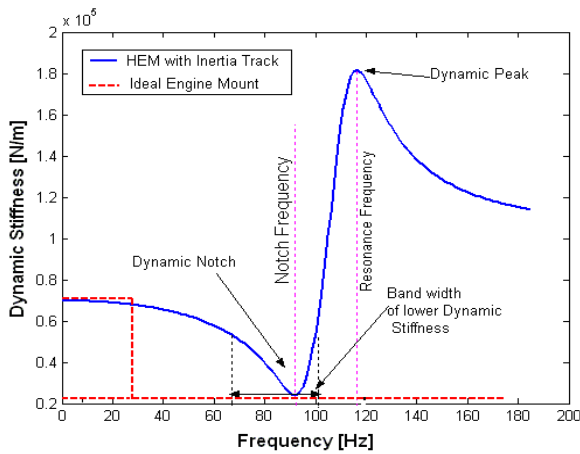


Fig.5 Dynamic Stiffness of HEM-IT

2.2.3 HEM with Inertia Track and Decoupler

HEM with Inertia track and decoupler (HEM-ITD), consists of two fluid-filled chambers connected through a decoupler and inertia track as shown in Fig.6. The decoupler plate has flexibility to travel within its cage. During floating condition of decoupler-plate, fluid flows freely. However once the plate rests in the cage, the fluid passes through the inertia track. In other words, during small amplitude excitations, the fluid passes freely through the decoupler from one chamber to other chamber, giving the low damping and stiffness characteristics. Fluid is forced through the inertia track during large amplitude vibrations, as the decoupler rest at bottom in its cage. To understand the complete dynamic behaviour of “HEM-ITD”, it is necessary to model this HEM. The lumped parameter model of HEM-ITD is shown in Fig.7a. F_{in} is the input excitation force from the engine side and F_T is the transmitted force to the chassis. A_p ($\sim 2500\text{mm}^2$) is the effective piston area which pumps the fluid from upper chamber to lower chamber. The k_r (225N/mm) and b_r ($0.1e3\text{Ns/m}$) are elastic stiffness and damping coefficient of upper chamber. C_1 ($2.5e-4 \text{ mm}^5/\text{N}$) and

C_2 ($2.5e-6 \text{ mm}^5/\text{N}$) are the compliance of the upper and lower chambers respectively.

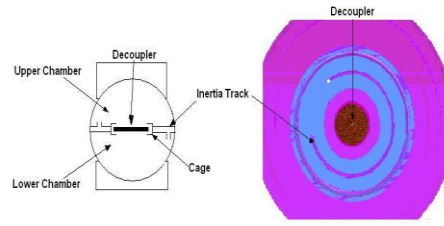


Fig.6 Schematic diagram of HEM-ITD

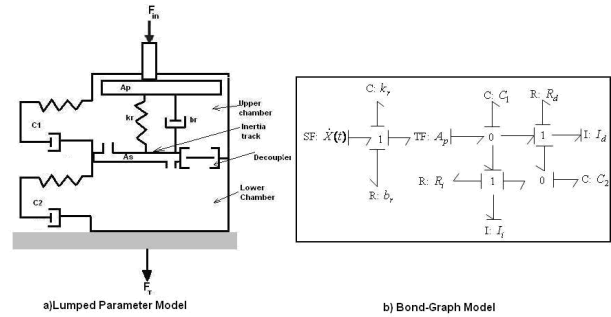


Fig.7 Lumped Parameter Model and Bond graph model of HEM-ITD

The bond graph diagram, which helps to derive mathematical differential equation, for the HEM-ITD is as shown in Fig.7b. In this bond graph, generalized variable ‘source of flow (SF)’, which is also known as power variable, has been used. In engine mount, this SF is the input to the system from engine which causes the flow inside the upper chamber. Along with the power variables, there are two more generalized variables called momentum $p(t)$ and displacement $Q(t)$. These are time integral of an effort and flow respectively. Terms 0 and 1 shows the 0-junction and 1 junction. In 0-junction the efforts are equal and algebraic sum of the flow is always zero (Thoma). In a 1-junction, the flows are equal and algebraic sum of effort is always zero (Thoma). The symbol \rightarrow is used to indicate the flow of energy. The upper chamber acts as piston A_p which is equivalent to a transformer function (TF). After the transformer function the flow differs which is indicated by 0-junction. The flow Q_i and Q_d is the inertia track flow and decoupler flow which shows inertia element (I) and the resistance element (R). C elements are the capacity or capacitance element.

The vibration at the top of the engine mount displaces the fluid of the top chamber. The displaced fluid by the piston area A_p causes the bulging of upper chamber as well as flow through the inertia track and decoupler. The bulging is taken care by the parameter compliance C_1 . The continuity equation for upper chamber becomes

$$C_1 \dot{P}_1 = A_p \dot{X} - Q_i - Q_d \tag{10}$$

Flow through the inertia track and decoupler enters the lower chamber which results in bulging of the lower chamber. The continuity equation of the lower chamber becomes

$$C_2 \dot{P}_2 = Q_i + Q_d \tag{11}$$

Flow through inertia track and decoupler occur because of the pressure difference between the upper and lower chambers. Therefore momentum equations for inertia track and decoupler are given by 12 and 13 respectively.

$$P_1 - P_2 = I_i \dot{Q}_i + R_i Q_i \tag{12}$$

$$P_1 - P_2 = I_d \dot{Q}_d + R_d Q_d \tag{13}$$

To simplify the problem, it is analyzed in two different domains (Singh, et al, 1992).The ‘free floating decoupler’ is characterized by low amplitude vibrations and ‘fixed decoupler’ is defined by high amplitude vibrations.

2.2.3 A. Free Floating Decoupler

Free floating condition of decoupler occurs when it does not contact the cage and almost complete flow passes freely through the decoupler, leaving negligible flow to pass through the inertia track ($Q_i=0$)(Singh, et al, 1992). The continuity equations 10 and 11, for small amplitude high frequency become,

$$C_1 \dot{P}_1 = A_p \dot{X} - Q_d \tag{14}$$

$$C_2 \dot{P}_2 = Q_d \tag{15}$$

and the momentum equation 12 and 13 gives,

$$P_1 - P_2 = I_d \dot{Q}_d + R_d Q_d \tag{16}$$

By reframing the equations derived from the Bond graph (Fig 7b) excitation force equation becomes,

$$F = k_r X + b_r \dot{X} + A_p P_1 \tag{17}$$

Let us assume that each system variable can be expressed by sinusoidal form as shown in Eq. (18). Such representation helps to express the equations of HEM-ITD in terms of input vibration amplitudes X and the disturbing frequency ω_{dr} .

$$\begin{aligned} P_1 &= \tilde{P}_1 e^{j\omega_{dr}t} \\ P_2 &= \tilde{P}_2 e^{j\omega_{dr}t} \\ Q_d &= \tilde{Q}_d e^{j\omega_{dr}t} \\ X &= \tilde{X} e^{j\omega_{dr}t} \end{aligned} \tag{18}$$

On differentiating with respect to time,

$$\begin{aligned} \dot{P}_1 &= j\omega_{dr} \tilde{P}_1 e^{j\omega_{dr}t} \\ \dot{P}_2 &= j\omega_{dr} \tilde{P}_2 e^{j\omega_{dr}t} \\ \dot{X} &= j\omega_{dr} \tilde{X} e^{j\omega_{dr}t} \end{aligned} \tag{19}$$

Now the continuity equation 14 becomes,

$$\begin{aligned} C_1 \dot{P}_1 &= A_p \dot{X} - Q_d \\ C_1 j\omega_{dr} \tilde{P}_1 e^{j\omega_{dr}t} &= A_p j\omega_{dr} \tilde{X} e^{j\omega_{dr}t} - \tilde{Q}_d e^{j\omega_{dr}t} \\ \tilde{P}_1 &= \frac{A_p}{C_1} \tilde{X} + j \frac{1}{\omega_{dr} C_1} \tilde{Q}_d \end{aligned} \tag{20}$$

Second continuity equation (Eq. 15),

$$\begin{aligned} C_2 \dot{P}_2 &= Q_d \\ C_2 j\omega_{dr} \tilde{P}_2 e^{j\omega_{dr}t} &= \tilde{Q}_d e^{j\omega_{dr}t} \\ \tilde{P}_2 &= -j \frac{1}{\omega_{dr} C_2} \tilde{Q}_d \end{aligned} \tag{21}$$

On substituting Eq. (20) and Eq. (21) into Eq. (16),

$$\begin{aligned} \frac{A_p}{C_1} \tilde{X} + j \frac{1}{\omega_{dr} C_1} \tilde{Q}_d + j \frac{1}{\omega_{dr} C_2} \tilde{Q}_d &= j\omega_{dr} I_d \tilde{Q}_d + R_d \tilde{Q}_d \\ \text{or } \frac{A_p}{C_1} \tilde{X} &= \left(R_d + j \left(I_d \omega_{dr} - \frac{1}{\omega_{dr} C_1} - \frac{1}{\omega_{dr} C_2} \right) \right) \tilde{Q}_d \\ \text{or } \tilde{Q}_d &= \frac{\frac{A_p}{C_1} \tilde{X}}{R_d + j \left(I_d \omega_{dr} - \frac{1}{\omega_{dr} C_1} - \frac{1}{\omega_{dr} C_2} \right)} \\ \text{or, } \tilde{Q}_d &= \frac{A_p C_2 \omega_{dr}}{R_d C_1 C_2 \omega_{dr} + j(I_d C_1 C_2 \omega_{dr}^2 - C_2 - C_1)} \tilde{X} \end{aligned} \tag{22}$$

Putting value of \tilde{Q}_d from equation 22 into the equations (20) and (21),

$$\tilde{P}_1 = \left(\frac{A_p}{C_1} + \frac{A_p C_2 j}{R_d C_1 C_2 \omega_{dr} + j(I_d C_1 C_2 \omega_{dr}^2 - C_1 C_2 - C_1^2)} \right) \tilde{X} \tag{23}$$

$$\tilde{P}_2 = \left(\frac{-A_p j}{R_d C_1 C_2 \omega_{dr} + j(I_d C_1 C_2 \omega_{dr}^2 - C_2 - C_1)} \right) \tilde{X} \tag{24}$$

Equations 23 and 24 give the pressures inside the upper and lower chamber respectively in terms of input displacement amplitude. Similarly, writing the equation of the applied force (Eq. 17) in terms of frequency, and putting the value of P_1 from equation (23),

$$\begin{aligned} \tilde{F} e^{j\omega_{dr}t} &= k_r \tilde{X} e^{j\omega_{dr}t} + j\omega_{dr} b_r \tilde{X} e^{j\omega_{dr}t} \\ &+ A_p \left(\left(\frac{A_p}{C_1} + \frac{A_p C_2 j}{R_d C_1 C_2 \omega_{dr} + j(I_d C_1 C_2 \omega_{dr}^2 - C_1 C_2 - C_1^2)} \right) \tilde{X} \right) e^{j\omega_{dr}t} \end{aligned}$$

On dividing the applied force \tilde{F} by \tilde{X} , the characteristic equation of dynamic stiffness, $K(\omega_{dr}, j)$

$$\begin{aligned} K(\omega_{dr}, j) &= k_r + j\omega_{dr} b_r + \frac{A_p^2}{C_1} \\ &+ \frac{A_p^2 C_2 j}{R_d C_1 C_2 \omega_{dr} + j(I_d C_1 C_2 \omega_{dr}^2 - C_1 C_2 - C_1^2)} \end{aligned} \tag{25}$$

The real part of the characteristic equation (25) is called as Dynamic stiffness.

Table1: Comparison of Engine Mount

Sr. No	Performance Zone	Low frequency large amplitude Vibrations (road excitations)	Low frequency low amplitude Vibrations (Engine idling)	High Frequency low amplitude Vibration (Engine running)	Remark
	Mount Type				
1 to 5 scale with 5 as the Best and 1 as worst.					
A	Elastomeric mount	3	2	2	Dynamic stiffness increases along with frequency
B	HEM with Orifice	4	3	3	Dynamic stiffness is almost constant
C	HEM with Inertia track	5	3	3	After Notch Frequency dynamic stiffness shows dynamic peak
D	HEM with inertia track and decoupler	5	5	3	High frequency Resonance of Dynamic Stiffness
E	Smart Mount	5	5	5	

2.2.3 B. Fixed Decoupler

It is expected that during large amplitude excitations the decoupler will spend the majority of time against the cage, and almost complete flow will pass through the inertia track. In such a situation terms Q_d and R_d will be equal to zero and equations 10 and 11 can be expressed in the following manner,

$$C_1 \dot{P}_1 = A_p \dot{X} - Q_i \tag{26}$$

$$C_2 \dot{P}_2 = Q_i \tag{27}$$

By converting these equations in frequency domain, it is possible to derive

$$K(\omega, j) = k_r + b_r \omega + \frac{A_p^2}{C_1} + \frac{C_2 A_p^2 j}{R_i C_1^2 C_2 \omega_{dr} + j(I_i C_1^2 C_2 \omega_{dr}^2 - C_2 C_1 - C_1^2)} \tag{28}$$

By using the dynamic stiffness Eq. (25) and Eq. (28), the graph plotted against the frequency is shown in Fig.8. In lower frequency zone, either decoupler or inertia track defines the property of the engine mount depending on the amplitude of excitation. During road excitations, fluid will flow through the inertia track giving higher values of the stiffness represented by the solid line (green colour). When the engine is idling without any disturbance from the road, the fluid will flow through the decoupler giving lower value of stiffness represented by dotted line (blue colour). It

solves the problem of the engine idle shake which was present in the HEM with inertia track. However, this figure indicates that the dynamic stiffness provided by the free decoupler exceeds the value given by inertia track. In the high frequency zone, the amplitudes of vibration are low therefore decoupler represents the property of the engine mount. In this condition, inertia track will not be active as the magnitude of excitations amplitude is low.

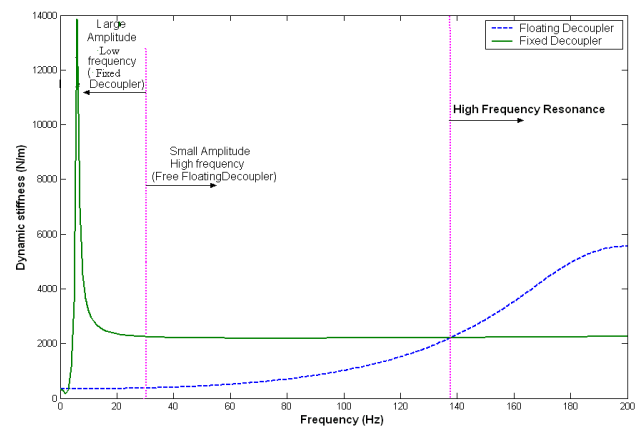


Fig. 8 Dynamic Stiffness of HEM –ITD

Thus it is observed that the HEM-ITD exhibit the high frequency resonance which is difficult to control as decoupler is sensitive only to amplitude, which is lower

in high frequency zone (Adiguna, et al, 2003), (Kim and Singh, 1995), (Colgate, et al, 1995). The HEM-ITD solves the problem of engine idling (2.2.3) if the assumptions of zero flow from inertia track during free decoupler and zero flow through decoupler during fixed decoupler are valid assumptions. However literature (Adiguna, et al, 2003), (Singh, 2007), (Ohadi and Maghsoodi, 2007) does not support practicality of these assumptions. In short, all three types of hydraulic mounts have limited operating range, as indicated in Table 1. The aim of the present paper is to target a smart mount which will perform similar to Ideal mount. Next subheading describes smart mounts to provide ideal behaviour from engine mount.

3. Smart Mount System

A typical architecture of a smart mount system is shown in Fig.9. Figure 9a shows a series combination of HEM and actuator, while Fig. 9b illustrates actuator as a part of HEM. This figure-9 indicates that signals from vibration sensors (mounted on chassis and engine) are passed to controller, which in turn instructs the actuator to counteract the vibrating energy. The vibration sensor may be a force sensor or an accelerometer. The controller adjusts the amplitude and phase of the force to be imposed by the actuator considering the behaviour of HEM to minimize the vibrations. Actuator adds or reduces the force applied against the input force offered by HEM. In the present design of smart mount, "HEM with inertia track" as basic structure has selected as it involves less number of non-linear parameters compared to the "HEM with inertia track and decoupler", therefore its control will be much easier.

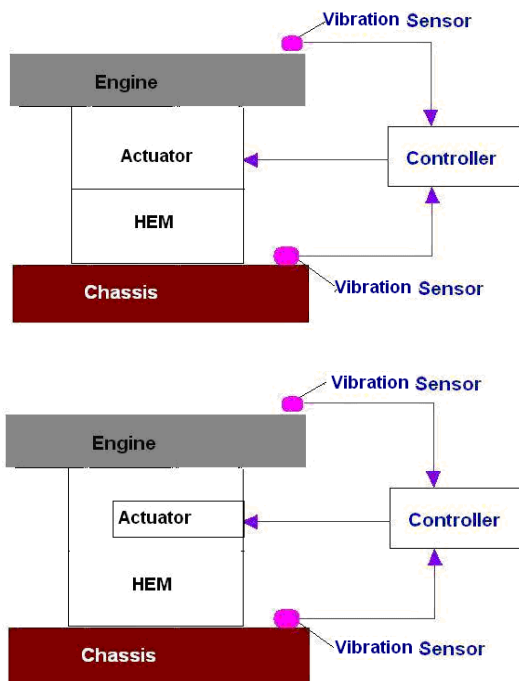


Fig. 9 Schematic representation of Smart Mount

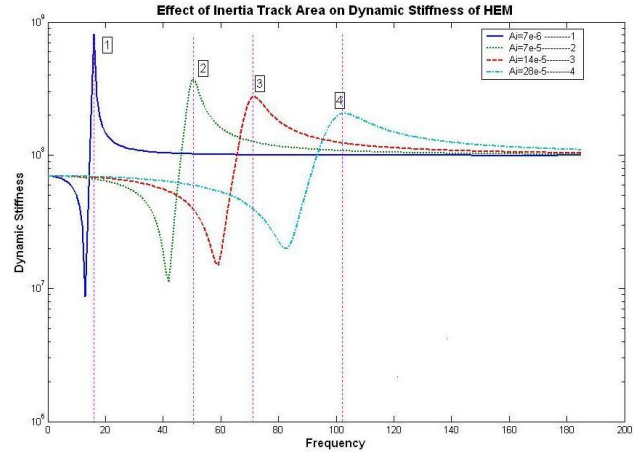


Fig. 10 Effect of Inertia track area on the Dynamic stiffness of HEM

The performance of the dynamic stiffness depends on the cross-sectional area of inertia track, which is given by equations 8 and 9. As it is very difficult to predict the behaviour of Inertia track area variation on the dynamic stiffness just by looking at the equations, MATLAB is used to plot the behaviour of the dynamic stiffness with area variation. The plot is as shown in the Fig. 10. This figure clearly shows that on increasing cross-sectional area of the inertia track, the peak values of dynamic stiffness decreases. Moreover increase in the area of inertia track shifts the 'peak' of dynamic stiffness toward the higher frequency zone. Thus by controlling the area, it is possible to control the dynamic 'notch frequency'.

Ahmadian and Kong, (1995) adopted a mechanism to control the area of inertia track. He explained the effect of complete closing of the inertia track on the dynamic stiffness. By putting the value of Inertia track equal to zero in equations 8 and 9, the characteristics equation of dynamic stiffness of closed HEM-IT becomes,

$$K_{closed}^* = (k_r + A_p^2 k_v) + j\omega_{dr}(b_r + A_p^2 b_v) \tag{29}$$

Closing of inertia track after the notch avoids the resonance peak as shown in fig 11. The dynamic stiffness of closed inertia track is almost constant throughout the frequency. Also at every frequency, the value of dynamic stiffness of closed inertia track HEM is greater than the HEM with open inertia track (Ahmadian and Kong, 1995), (Kong, et al, 2005). As per Ahmadian and Kong, (1995) during the lower frequencies where amplitudes are larger, the closed valve condition provides higher dynamic stiffness and in higher frequency range (till the notch frequency), open valve offers lesser dynamic stiffness. At frequency greater than notch frequency again closed valve position is preferred to avoid the resonance peak (Ahmadian and Kong, 1995). To turn on and off the valve (Ahmadian and Kong, 1995) used a controllable Magneto Rheological Fluid (MRF). The fluid needs minimum energy i.e. magnetic induction of 1.3-2.0

Tesla which can be produced by 12V battery and minimum time (30msec) to respond to signal. Effort made by Ahmadian and Kong (1995) is appreciable, but still the performance of the mount does not match the performance of ideal mount. Engine idling and the performance after the notch frequency deviates from that of ideal mount.

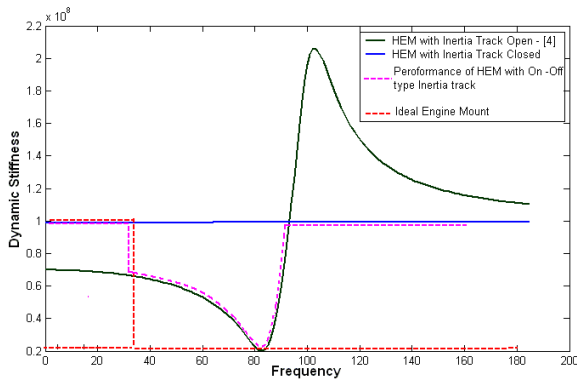


Fig. 11 Effect of Closed Inertia track on the Dynamic stiffness of HEM

3.1 Design Concept of Smart Mount

Study in previous paragraphs indicates that the dynamic notch and the resonance peak can be controlled by varying the area of inertia track area. In the present study controlling the area of inertia track has been targeted and mount which has such features is named as “Smart mount”. Figure 12 shows that a close control on the area provides dynamic stiffness (shown by blue dotted line) approaching to the dynamic stiffness of idle mount. The transmissibility curves for Smart Mount, shown by blue dotted line, are plotted in fig.13. The red dotted line shows the performance of the ideal mount. These two figures (Figs. 12-13) encourage designing an engine mount having continuous control on the area of inertia track area. Such a design is explained in sub-section.

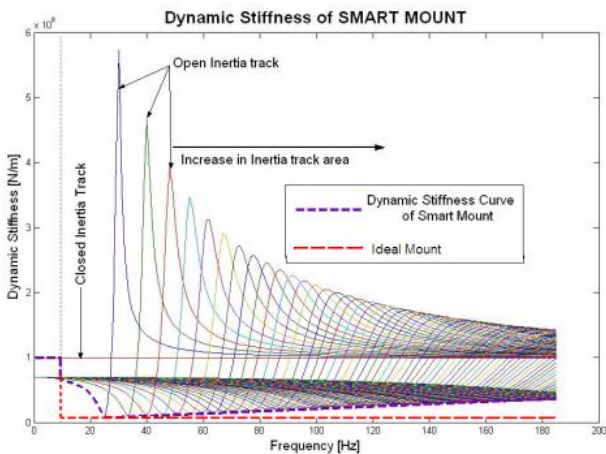


Fig. 12 Dynamic stiffness with Variable Inertia Track Area

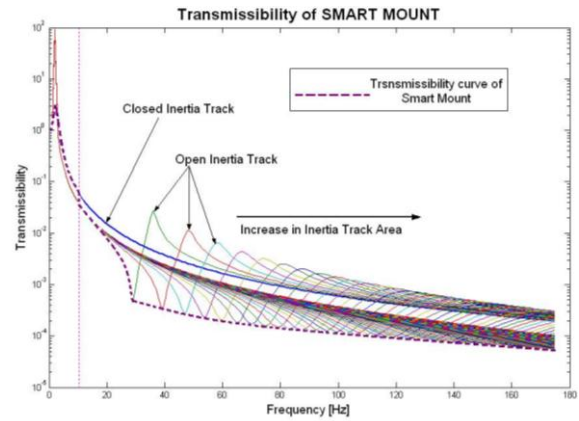


Fig. 13 Transmissibility with Variable Inertia Track Area

3.1.1 Variable Area of Inertia Track

In the present study, two concepts to dynamically controlled area of inertia track have been evolved. The first concept is to provide a valve on the inertia track which will be controlled by the sensors and the controller. To provide a valve on the inertia track is again a difficult task as inertia track is a part of mid housing and located inside the HEM. To solve this problem, HEM with external inertia track is useful solution. The schematic representation of the first concept is as shown in fig.14. This involves a valve which is fitted on the inertia track, a controller mechanism which will operate the valve. This concept requires extra space compared to elastomeric and hydraulic mounts. The fitment of the valve on the inertia track is again a difficult task as inertia track is very small in diameter (1.5 to 3mm ID). External inertia track if fitted with a small valve again has a drawback or reliability as it is prone to the leakages through the joineries. This concept in thus put a question marks on its application. The target is to now change the small area of the track without putting any additional part on it.

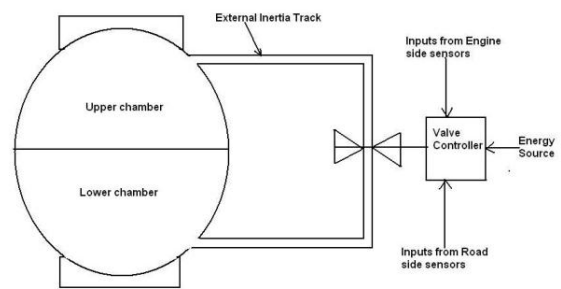


Fig. 14 Schematic valve mechanism for controlling area of inertia track Concept 1

To overcome the problem, the second concept is hypothesized, which is shown in fig.15. In this concept, the controllable MR fluid (MRF132) is filled inside the mount. External inertia track is passed through the core of the electromagnet. The change in value of

electric current supplied to electromagnet varies the magnet field (Li, et al, 1999) and affects the MRF particle chains. These chains restrict the movement of the fluid and thereby vary the shear strength of the suspension. MR fluids routinely exhibit shear strengths ranging between 50 to 100 kPa (Carlson) for applied magnetic field of 150 - 250 kA / m (for magnetic induction of 1.3-2.0 Tesla). The behaviour of such a controllable fluid is often represented as a Bingham plastic having variable shear strength.

$$\tau = \tau_{ys} + \eta \dot{\gamma} \tag{30}$$

Where yield stress, τ_{ys} , is expressed by

$$\tau_{ys} = 6^{1/2} * \phi * \mu_o * M_s^{1/2} * H^{3/2} \tag{31}$$

The relationship between the magnetic field intensity (H), and voltage (V) is given by

$$H = nI \tag{32} \quad H = n * \frac{V * \pi * D^2}{4 * \rho Cu * l} \tag{33}$$

By putting the value of magnetic field intensity from equation 33 into equation 31, the relationship between the yield stress and voltage is given as,

$$\tau_{ys} = 6^{1/2} * \phi * \mu_o * M_s^{1/2} * \left(n * \frac{V * \pi * D^2}{4 * \rho Cu * l} \right)^{3/2} \tag{34}$$

This equation indicates that increasing value of V increases τ_{ys} , which in turn increases the resistance against fluid flow. Such physical effect can be analyzed using ‘valve mode’ mechanism (Carlson).

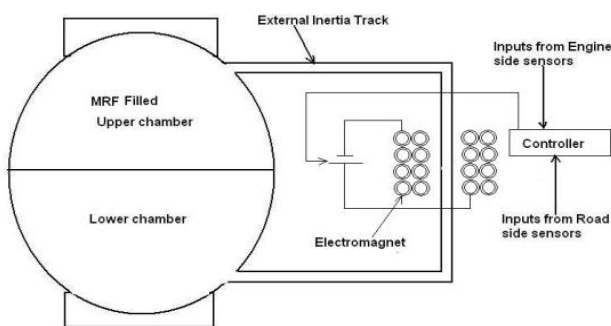


Fig. 15 Schematic valve mechanism for controlling area of inertia track Concept 2

To apply the concept of hardening of MR fluid on engine mount let us consider the displacement applied either at the base or at the top of the engine mount, which in turn vary the pressure inside the chambers. The pressure difference can be expressed in terms field independent viscous component (White, 1994) and field induced yield stress component (Carlson), such as, Field Independent Component,

$$\Delta P_{\eta} = \frac{32 \mu L_i Q_i}{\rho g A_i} \tag{35}$$

Field Dependent Component,

$$\Delta P_{\tau} = \frac{c \tau_{ys} L_i}{g} \tag{36}$$

Where,

$$c = 2 \quad \text{for} \left(\frac{\Delta P_{\tau}}{\Delta P_{\eta}} \right) < 1 \tag{37}$$

$$c_{\max} = 3 \quad \text{for} \left(\frac{\Delta P_{\tau}}{\Delta P_{\eta}} \right) > 3$$

In case of normal fluids used for HEM, the pressure difference which causes the flow is given by the Eq. (35). In case of different types of HEM, the less stiffness is produced by less restricted flow across the chambers. This effect can be produced by larger area of the inertia track and less viscosity of the fluid. For getting the higher stiffness of the mount the restriction to the flow across the chambers should be more. This effect is produced by the lesser area for flow and higher viscosity of the fluid.

The behaviour of the pressure difference across two chambers with variation of the magnetic field intensity, expressed in Eq. 36, is shown in Fig 16. It shows that the pressure difference between upper chamber and lower chamber increases along with the increase in the yield stress of the MRF passing through the inertia track. At the saturation limit of MRF, the fluid becomes solid and the MRF based smart mount will act as elastomeric mount which will support the road shocks. By reducing the intensity of magnetic field (i.e. by reducing the applied voltage to the electromagnet), the mount stiffness can be reduced to achieve the dynamic notch.

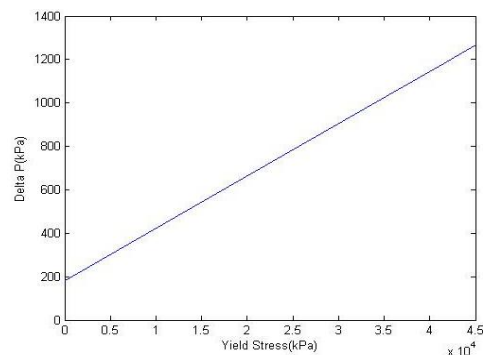


Fig. 16 Delta P as a function of yield stress

By summing Eqs. (35-36), total pressure drop is expressed as,

$$\Delta P = \frac{32 \mu L_i Q_i}{\rho g A_i} + \frac{c \tau_{ys} L_i}{g} \tag{38}$$

This equation shows that increasing τ_{ys} and decreasing A_i the pressure difference increases. The behaviour of

pressure difference across chambers is plotted against the change in area of inertia track as shown in Fig. 17. These results indicate that MRF-based engine mounts perform as good as an ideal engine mount.

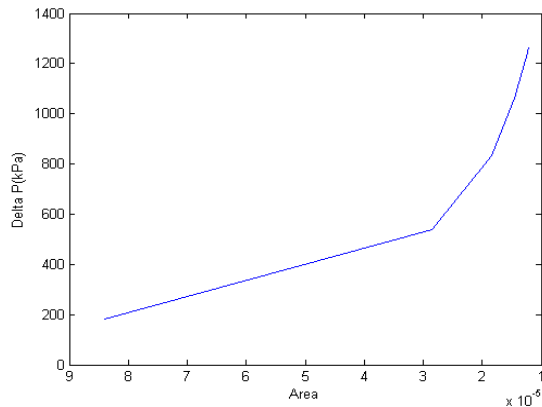


Fig. 17 Delta P as a function of area of inertia track

Conclusions

In the present study, the performance requirements from an ideal engine mount have been detailed. Commonly used elastomeric and hydraulic mounts have analyzed, and compared with smart engine mount. The design and analysis of Magnetorheological fluid (MRF) based engine mount have been described. The results of dynamic stiffness and transmissibility of MRF-smart mount have been compared with ideal engine mount. Finally it can be concluded that:

- Hydraulic mount with inertia track can be used as MRF-smart mount by replacing hydraulic fluid with Magnetorheological fluids, and
- Dynamic stiffness and transmissibility of MRF-smart mount is equivalent to the performance required from an ideal mount. Therefore MRF-mount can be treated as an “ideal engine mount”.

References

- A. R. Ohadi, G. Maghsoodi, (2007), Simulation of engine vibration on nonlinear hydraulic engine mounts, *Journal of Vibration and Acoustics*, 129, pp. 417-424.
- C. Sarkar, H. Hirani, (2013), Theoretical and experimental studies on a magnetorheological brake operating under compression plus shear mode, *Smart Materials and Structures*, 22, art. no. 115032.
- C. Sarkar, H. Hirani, (2013), Synthesis and characterization of antifriction magnetorheological fluids for brake, *Defence Science Journal*, 63, pp. 408-412.
- C. Sarkar, H. Hirani, (2013), Design of a squeeze film magnetorheological brake considering compression enhanced shear yield stress of magnetorheological fluid, *Journal of Physics: Conference Series*, 412, 012045.
- C. Sarkar, H. Hirani, (2015), Synthesis and characterization of nano-copper-powder based magnetorheological fluids for brake, *International Journal of Scientific Engineering and Technology*, 4, pp. 76-82.
- C. Sarkar, H. Hirani, (2015), Effect of particle size on shear stress of magnetorheological fluids, *Smart Science*, (in press).
- C. Sarkar, H. Hirani, (2015), Development of magnetorheological brake with slotted disc, *Proc. IMechE, Part D: Journal of Automobile Engineering*, (in press).
- D. Carlson, D. Catanzarite, K. Clair, Commercial magneto-rheological fluid devices, *Lord Corporation*. www.lord.com.
- F. M. White, (1994), *Fluid Mechanics*, McGraw-Hill, Inc., Toronto.
- G. Kim, R. Singh, (1995), A study of passive and adaptive hydraulic engine mount systems with emphasis on non-linear characteristics. *Journal of Sound and Vibration*, 179, pp 427-453.
- H. Hirani, C. S. Manjunatha, (2007), Performance evaluation of magnetorheological fluid variable valve, *Proc. of the Institution of Mechanical Engineers, Part D, Journal of Automobile Engineering*, 221, pp. 83-93.
- H. Adiguna, M. Tiwari, R. Singh, H. Tseng, D. Hrovat, (2003), Transient response of a hydraulic engine mount, *Journal of Sound and Vibration*, 268, pp 217-248.
- J. Thoma, *Simulation by bond-graphs*, Springer-Verlag publications, ISBN0-387-51640-9.
- J. Colgate, C. Chiou, W. Liu, L. Keer, (1995), Modelling of hydraulic engine mount focusing on response to sinusoidal and composite excitations, *Journal of Sound and Vibration*, 184, pp.503-528.
- J. Venezia, (1997), *Vibration modelling and experimental analysis of a locomotive cab*, Master Thesis, Virginia Polytechnic Institute and State University.
- M. Ahmadian, Y. Kong, (1999), Performance analysis of magneto rheological mounts, *Journal of Intelligent Material Systems and Structures*, 10, pp.248-256.
- M. Bernuchon, (1984), A new generation of engine mount. *SAE Technical Paper*, 840259.
- M. D. Rao, S. Gruenberg, D. Griffiths, (2001), Measurement of dynamic parameters of automotive exhaust hanger, *Society of Automotive Engineers*, 01NVC-121 (8pp).
- M. J. M. Gomes, A. S. Pouzada, (2002), Dynamic behaviour of rubber compounds for engine mounts, *Key Engineering Materials*, 230-232, pp. 303-306.
- P. E. Corcoran, G. H. Ticks, (1984), Hydraulic engine mount characteristics, *SAE Technical Paper*, 840407.
- P. R. Choudhury, (2004), *Workshop on Dynamic Testing of Rubber Sample and Rubber Products for Automobile Industry*, May.
- R. Singh, (2000), Dynamic design of automotive systems: Engine mounts and structural joints, *Sadhana*, 25, pp. 319-330.
- R. Singh, (2007), Anatomy of a Real-Life Non-Linear Device: Hydraulic Engine Mount, *International Modal Analysis Conference, Orlando, FL*.
- R. Singh, G. Kim, P. Ravindra, (1992), Linear analysis of automotive hydraulic-mechanical mount with emphasis on decoupler characteristics. *Journal of Sound and Vibration*, 158, pp.219-243.
- Regis, (1976), Charles design of elastomeric vibration isolation mounting system for internal combustion engines, *SAE Technical Paper*, 760431.
- S. Gupta, H. Hirani, (2011), Optimization of magnetorheological brake, *ASME/STLE 2011 International Joint Tribology Conference*, pp 405-406.
- T. Q. Thanh, K. Kwan, Y. Kong, (2006), Optimal parameter control for multi-signal of semi-active engine mount, *The 1st International Forum on Strategic Technology (IFOST)*, pp. 20-23.
- T. Ushijima, K. Takano, H. Kojima, (1998), High performance hydraulic mount for improving vehicle noise and vibration, *SAE Technical Paper Series*, 880073.
- V. K. Sukhwani, V. Lakshmi, H. Hirani, (2006), Performance evaluation of MR brake: an experimental study, *Indian Journal of Tribology*, pp. 67-52.
- V. K. Sukhwani, H. Hirani, T. Singh, (2007), Synthesis of magnetorheological grease, *Greasetech India*.
- V. K. Sukhwani, H. Hirani, (2007), Synthesis and characterization of low cost magnetorheological (MR) fluids, *The 14th International Symposium on: Smart Structures and Materials & Nondestructive Evaluation and*
- V. K. Sukhwani, H. Hirani, (2008), A comparative study of magnetorheological-fluid-brake and magnetorheological-grease-brake, *Tribology Online*, 3, pp. 31-35.
- V. K. Sukhwani, H. Hirani, T. Singh, (2008), Synthesis and performance evaluation of MR grease, *NLGI Spokesman*, 71.
- V. K. Sukhwani, H. Hirani, (2008), Design, development and performance evaluation of high speed MR brake, *Proc. Institute Mech. Engineers., Part L, Journal of Materials: Design and Applications*, 222, pp.73-82.
- V. K. Sukhwani, H. Hirani, T. Singh, (2009), Performance evaluation of a magnetorheological grease brake, *Greasetech India*, 9, pp. 5-11.
- Y. Yu, S. Peelamedu, N. Naganathan, R. Dukupati, (2001), Automotive vehicle engine mounting systems: A survey, *Journal of Dynamic Systems, Measurement, and Control*, 123, pp.186-194.
- Y. Kong, Y. Kim, B. Yang, M. Ahmadian, (2005), Optimal design of engine mount using an enhanced genetic algorithm with simplex method, *Vehicle System Dynamics*, 43, pp. 57-81.
- W. C. Flower, (1985), Understanding hydraulic mounts for improved vehicle noise, vibration and ride qualities, *SAE Technical Paper*, 850975.
- W. H. Li, G. Chen, S. Yeo, (1999), Viscoelastic properties of MR Fluids, *Smart Materials and Structures*, 8, pp. 460-468.